

# Topology-Preserving Loss for Accurate and Anatomically Consistent Cardiac Mesh Reconstruction

Chenyu Zhang<sup>1,\*</sup>, Yihao Luo<sup>1,\*</sup>, Yinzhe Wu<sup>1</sup>, Choon Hwai Yap<sup>1,†</sup>, Guang Yang<sup>1,2,3,†</sup>

<sup>1</sup> Bioengineering Department Imperial College London, London W12 7SL, United Kingdom

{chenyu.zhang24,y.luo23,yinzhe.wu18,c.yap}@imperial.ac.uk

<sup>2</sup> National Heart and Lung Institute, Imperial College London, London, United Kingdom

<sup>3</sup> School of Biomedical Engineering & Imaging Sciences, King's College London, London, United Kingdom

g.yang@imperial.ac.uk

\* These authors contributed equally to this work.

† Co-last and senior authors.

**Abstract.** Accurate cardiac mesh reconstruction from volumetric data is essential for personalized cardiac modeling and clinical analysis. However, existing deformation-based approaches are prone to topological inconsistencies, particularly membrane penetration, which undermines the anatomical plausibility of the reconstructed mesh. To address this issue, we introduce Topology-Preserving Mesh Loss (TPM Loss), a novel loss function that explicitly enforces topological constraints during mesh deformation. By identifying topology-violating points, TPM Loss ensures spatially consistent reconstructions. Extensive experiments on CT and MRI datasets show that TPM Loss reduces topology violations by up to 93.1% while maintaining high segmentation accuracy (DSC: 89.1%-92.9%) and improving mesh fidelity (Chamfer Distance reduction up to 0.26 mm). These results demonstrate that TPM Loss effectively prevents membrane penetration and significantly improves cardiac mesh quality, enabling more accurate and anatomically consistent cardiac reconstructions. The implementation is publicly available at GitHub Repository.

**Keywords:** Topology-preserving Loss · Cardiac Reconstructions · Deformation.

## 1 Introduction

Accurate and topologically consistent 3D cardiac mesh reconstruction is crucial for simulate various aspects of cardiac function, particularly in tissue mechanics [12], electrophysiology [17], and personalized cardiac interventions. As shown in Fig.1(a), standard deformation-based approaches often introduce extraneous

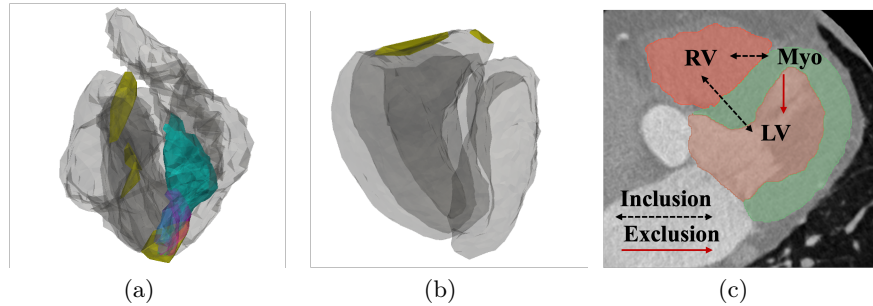


Fig. 1: Comparison of topology-aware and topology-agnostic results in both 2D and 3D representations. **(a)** 3D Mesh without Topology Constraints, **(b)** 3D Mesh with Topology-Preserving Constraints, **(c)** 2D Ground Truth Label with Topology Information, The gray regions represent the anatomical structures, while the cyan and magenta areas highlight the intersection regions between different anatomical components. The yellow regions indicate areas where one structure has abnormally penetrated another, violating anatomical constraints.

regions containing topological anomalies, such as membrane penetration and unnatural inter chamber connections, violating anatomical constraints and resulting in physiologically implausible geometries. These regions introduce risks in downstream applications, including hemodynamic simulations [13] and patient-specific treatment planning [7].

Traditional deformation-based reconstruction methods employ deep learning techniques to extract cardiac structures from volumetric data [8,2,11], but they lack explicit mechanisms to enforce topology preservation. Prior works [1,15] have attempted to improve topological consistency through voxel-based topology constraints, but these approaches operate at the segmentation level and do not directly optimize mesh topology. Similarly, standard mesh regularization techniques, such as Chamfer distance [5] and Laplacian smoothing [14], focus on improving geometric smoothness but fail to prevent crucial topological errors. While occupancy-based method have shown promise in shape reconstruction [9,10], they lack explicit multi-class anatomical constraints, making them insufficient for complex cardiac modeling.

To address this, a loss function must not only guide shape refinement but also encode explicit multi-class anatomical constraints at the mesh level. We propose Topology-Preserving Mesh Loss (TPM Loss), which directly integrates topological consistency into the optimization process, ensuring spatially plausible reconstructions. Our approach is based on three key innovations:

1. Topology Interaction Module – We introduce a topology-aware constraint mechanism that systematically identifies and penalizes membrane penetration and inter-chamber connectivity errors, preventing unintended structural overlaps.

2. Topological refinement based on occupancy - We leverage winding-based occupancy verification to dynamically refine mesh deformations, ensuring that the reconstructed surface adheres to anatomical boundaries while eliminating topology violations.
3. Quantifiable Topology Preservation – Unlike previous works that focus solely on Dice score and Chamfer Distance, we introduce a dedicated Topology Violation Score (TVS) to rigorously evaluate topological consistency.

## 2 Methodology

In this section, we propose Topology-Preserving Mesh Loss (TPM Loss) to enforce topological consistency in cardiac mesh reconstruction. Our method extends previous topology-aware constraints from 2D segmentation to 3D cardiac meshes, ensuring anatomical relationships are preserved at the mesh level. Additionally, we introduce a multi-class occupancy formulation, improving traditional winding occupancy verification, which lacks explicit inter-chamber constraints. Furthermore, we define a dedicated topology evaluation metric to quantify topology violations and enable objective comparisons with prior methods.

### 2.1 Topological Interaction Module

Inspired by [6], we introduce a topological interaction module that enforces anatomical constraints by defining inclusion and exclusion rules between cardiac structures. The interaction rule set  $\mathcal{R}$  specifies the expected spatial relationships:

$$\mathcal{R} = \{(A_i, A_j, T_{ij})\} \quad (1)$$

where  $A_i$  and  $A_j$  denote different cardiac structures, and  $T_{ij}$  determines whether  $A_i$  should be inside  $A_j$  or separate. When  $T_{ij} = 1$ ,  $A_i$  should be enclosed within  $A_j$ , as in the case of the blood pool inside the myocardium. When  $T_{ij} = 0$ ,  $A_i$  and  $A_j$  must not overlap, ensuring distinct anatomical boundaries such as the separation of LV and RV, as shown in Fig .1(c).

Using these constraints, we define voxel-based topology validation using a binary kernel  $K$  which is 6-connected. Given a binary segmentation  $P$ , we compute neighborhood overlap for each label pair  $(A_i, A_j)$ :

$$N_{A_j} = P(A_j) * K, \quad (2)$$

where  $*$  denotes 3D convolution.

For exclusion constraints, where  $A_i$  and  $A_j$  should remain separate, violations occur when  $A_i$  appears within the neighborhood of  $A_j$ . Conversely, for inclusion constraints, where  $A_i$  should be inside  $A_j$ , violations are detected when  $A_i$  extends beyond  $A_j$ :

$$V_{A_i} = (P = A_i) \cap N_{A_j}, V_{A_i} = (P = A_i) \cap (1 - N_{A_j}), \quad (3)$$

where  $1 - N_{A_j}$  represents the exterior of  $A_j$ . By aggregating these violation maps, we construct a critical voxel map  $V$ , which identifies erroneous regions in the segmentation.

## 2.2 Critical Voxel Point Cloud Representation

To integrate topology-aware constraints into mesh deformation, we convert the critical voxel map  $V$  into a point cloud representation:

$$P_{\text{vio}} = \{(\mathbf{T}(i, j, k, 1), A_i) \mid V(A_i, i, j, k) = 1\}, \quad (4)$$

where  $(i, j, k)$  are the voxel indices, and  $\mathbf{T}$  is the affine transformation matrix derived from the imaging metadata that encodes voxel spacing, orientation, and patient positioning to convert discrete voxel indices into real-world spatial coordinates.

## 2.3 Occupancy-Based Mesh Optimization

In order to ensure topological constraints are explicitly preserved in cardiac mesh reconstruction, we introduce a multi-class occupancy formulation. The key idea is to evaluate the occupancy function  $O(p)$  for a set of query points  $p \in \mathcal{Q}$ , which determines whether a given point is inside or outside a cardiac structure[9].

$$O(p) = \frac{1}{4\pi} \sum_{v \in V} A_v \cdot \frac{(p-v)}{\|p-v\|^3}, \quad (5)$$

where  $A_v$  is the dual area weight of vertex  $v$ , and  $\|p-v\|^3$  represents the cubed Euclidean distance between  $p$  and  $v$ . And, the normalization factor  $\frac{1}{4\pi}$  originates from the Poisson surface representation, ensuring a physically meaningful and consistent estimation of the occupancy state.

The function aggregates contributions from all mesh vertices, weighted by their dual area and inversely scaled by the cube of their Euclidean distance to the query point. Intuitively,  $O(p)$  acts as a potential field that allows distinguishing between the interior and exterior regions, providing a robust and differentiable constraint for the reconstruction of the mesh with a topological consistency.

**Composition of query points** To ensure anatomical consistency, query points are sampled from the ground truth and classified as positive or negative. These points guide mesh reconstruction by enforcing both segmentation accuracy and topological validity. If topological constraints are not considered, the classification relies solely on occupancy consistency, forming the basis of  $\mathcal{L}_{\text{occ}}$ , which ensures that the reconstructed mesh aligns with the underlying anatomy without explicitly enforcing inter-structure relationships.

For a given anatomical structure  $A_i$ , the classification is adapted to incorporate topological constraints: positive samples include points labeled as  $A_i$  in the ground truth, while negative samples not only include points from other structures or the background but also additional topology-aware modifications to enforce anatomical consistency.

$$S_{A_i}^+ = \{p \in \mathbb{R}^3 \mid L(p) = A_i\}, S_{A_i}^- = \{p \in \mathbb{R}^3 \mid L(p) \neq A_i\}, \quad (6)$$

where  $L(p)$  represents the ground truth label at point  $p$ ,  $S_{A_i}^+$  denotes the positive sample set, and  $S_{A_i}^-$  represents the negative sample set. If  $A_i$  is subject to a topological constraint, these sets are adjusted to enforce anatomical consistency.

*Exclusion Constraints* An exclusion constraint ensures that  $A_i$  and  $A_j$  remain spatially disjoint, preventing overlap. Violations are added to the negative sample set, while positive samples remain unchanged, consisting of standard points from  $A_i$ . The negative sample set includes both global negatives and overlapping points from  $A_j$ , defined as:

$$S_{A_i}^- = S_{A_i}^- \cup S^- A_i^{\text{exc}}, \quad S^- A_i^{\text{exc}} = \{P_{\text{vio}} \mid P_{\text{vio}} \in A_j, P_{\text{vio}} \in N_{A_i}\}, \quad (7)$$

*Inclusion Constraints* An inclusion constraint ensures that  $A_i$  is fully contained within  $A_j$ , preventing boundary violations. Sample selection is adjusted accordingly, with positive samples including both standard points from  $A_i$  and enclosing points from  $A_j$ , denoted as:

$$S_{A_i}^+ = S_{A_i}^+ \cup S^+ A_i^{\text{inc}}, \quad S^+ A_i^{\text{inc}} = \{P_{\text{vio}} \mid P_{\text{vio}} \in A_j, P_{\text{vio}} \in N_{A_i}\}, \quad (8)$$

Negative samples include points from outside  $A_i$  and additional points from  $A_i$  that incorrectly extend beyond  $A_j$ :

$$S_{A_i}^- = S_{A_i}^- \cup S^- A_i^{\text{inc-vio}}, \quad S^- A_i^{\text{inc-vio}} = \{P_{\text{vio}} \mid P_{\text{vio}} \in A_i, P_{\text{vio}} \notin N_{A_j}\}, \quad (9)$$

**Occupancy Loss for Mesh Optimization** The TPM Loss optimizes the reconstructed mesh by enforcing anatomical validity through occupancy constraints and cross-entropy loss. Cross-entropy loss is chosen because it directly optimizes per-point classification, making it well-suited for mesh-based learning tasks. Unlike region-based losses such as Dice loss, cross-entropy provides stable gradients even when class distributions are imbalanced or when anatomical structures vary significantly in size. In practice, we observed that using Dice loss instead of cross-entropy resulted in less stable training dynamics, making convergence more challenging,

$$\mathcal{L}_{\text{TPM}} = -\frac{1}{N} \sum_p O_{\text{gt}}(p) \log O(p) + (1 - O_{\text{gt}}(p)) \log(1 - O(p)), \quad (10)$$

where  $O(p)$  is the predicted occupancy,  $O_{\text{gt}}(p)$  is the ground truth. The ground truth occupancy follows:

$$O_{\text{gt}}(p) = \begin{cases} 1, & p \in S_{A_i}^+ \\ 0, & p \in S_{A_i}^- \end{cases}. \quad (11)$$

## 2.4 Overall Loss

The loss function optimizes the reconstructed mesh by enforcing anatomical validity, geometric accuracy, and topological consistency. It consists of several terms:

$$\mathcal{L} = \mathcal{L}_{\text{ce}} + \mathcal{L}_{\text{occ}} + \lambda_{\text{TP}} \mathcal{L}_{\text{TPM}}, \quad (12)$$

where  $\mathcal{L}_{ce}$  is the cross-entropy loss for segmentation,  $\mathcal{L}_{occ}$  ensures consistency in the reconstructed mesh,  $\mathcal{L}_{TP}$  penalizes violations of predefined topological constraints. Unlike  $\mathcal{L}_{ce}$  and  $\mathcal{L}_{occ}$ , which naturally align in numerical scale and contribute directly to mesh segmentation consistency,  $\mathcal{L}_{TPM}$  enforces global topological constraints. To prevent topology preservation from dominating the optimization or being underemphasized, we introduce  $\lambda_{TP}$  as a balancing factor, which is further analyzed in the experimental section.

## 2.5 Topology Evaluation Metric

To assess topology preservation, we define the Topology Violation Score (TVS) as

$$\text{TVS} = \frac{\sum_{i,j} |\mathcal{I}_{i,j}| + |\mathcal{O}_i|}{\sum_i |\mathcal{V}_i|}, \quad (13)$$

where  $\mathcal{I}_{i,j}$  denotes the intersection region between structures  $i$  and  $j$ ,  $\mathcal{O}_i$  is the region of structure  $i$  extending beyond its enclosing structure, and  $\mathcal{V}_i$  denotes the total anatomical reference volume.

## 3 Experimental analysis

To evaluate the effectiveness of the proposed TPM Loss, we conduct experiments using a deep learning-based mesh reconstruction framework. The framework consists of the 3D U-Net [20] for multi-scale feature extraction, coupled with the Graph Convolutional Network (GCN) [4] to model mesh topology and enforce spatial coherence. We aim to test whether incorporating topological constraints improves the anatomical consistency of reconstructed cardiac meshes without significantly compromising segmentation accuracy. By comparing models trained with and without TPM Loss, we hypothesize that topology-aware constraints will lead to a substantial reduction in topology violations, as measured by the Topology Violation Score (TVS), while maintaining competitive Dice Similarity Coefficient (DSC) and Chamfer Distance (CD) performance. Furthermore, we investigate the impact of different values of  $\lambda_{TP}$  to determine the optimal balance between geometric fidelity and topological correctness.

### 3.1 Datasets, models, and performance evaluation

We evaluate TPM Loss on multi-modal datasets (CT: MMWHS[19], WHS++[18], CCT48[16]; MRI: MMWHS[19], WHS++[18], ACDC[3]) with varying resolutions (0.78–1.68 mm in-plane, 1.6–10 mm slice thickness). CT datasets provide higher-resolution structural details, while MRI datasets exhibit greater anatomical variability, making them ideal for assessing generalization.

To ensure stable training, we first optimize the model using  $\mathcal{L}_{Dice} + \mathcal{L}_{occ}$  before introducing  $\mathcal{L}_{TP}$ . All implementation details, including hyperparameters, data preprocessing, and training configurations, are made publicly available in our GitHub repository for reproducibility.

Table 1: Quantitative comparison of TPM Loss ( $\lambda_{\text{TP}}$ ) on CT datasets. Higher DSC and lower CD and TVS indicate better performance. The values in parentheses represent the change compared to  $\lambda_{\text{TP}} = 0$ , where **red** indicates an increase and **green** indicates a decrease.

Dataset	$\lambda_{\text{TP}}=0$			$\lambda_{\text{TP}}=0.5$			$\lambda_{\text{TP}}=1$		
	DSC $\uparrow$ (%)	CD $\downarrow$ (mm)	TVS $\downarrow$	DSC $\uparrow$ (%)	CD $\downarrow$ (mm)	TVS $\downarrow$	DSC $\uparrow$ (%)	CD $\downarrow$ (mm)	TVS $\downarrow$
MMWHS	<b>92.3</b>	0.35	0.0627	91.8 (-0.5)	<b>0.14</b> (-0.21)	<b>0.0054</b> (-91.4%)	87.9 (-4.4)	0.47 (+0.12)	0.0061 (-90.3%)
WHS++	<b>91.7</b>	0.41	0.0701	90.1 (-1.6)	<b>0.36</b> (-0.05)	<b>0.0053</b> (-91.0%)	88.3 (-3.4)	0.38 (-0.03)	0.0068 (-90.3%)
CCT48	<b>94.2</b>	0.92	0.0524	92.9 (-1.3)	0.80 (-0.12)	<b>0.0051</b> (-90.3%)	90.8 (-3.4)	<b>0.64</b> (-0.28)	0.0054 (-89.7)

We assess reconstruction quality using Dice Similarity Coefficient (DSC), Chamfer Distance (CD), and Topology Violation Score (TVS). DSC measures segmentation accuracy by evaluating mesh overlap with the ground truth, while CD quantifies geometric fidelity based on nearest-point distances. Unlike these metrics, TVS explicitly captures topology errors such as chamber intersections and containment violations.

Table 2: Quantitative comparison of TPM Loss ( $\lambda_{\text{TP}}$ ) on MRI datasets. Higher DSC and lower CD and TVS indicate better performance. The values in parentheses represent the change compared to  $\lambda_{\text{TP}} = 0$ , where **red** indicates an increase and **green** indicates a decrease.

Dataset	$\lambda_{\text{TP}}=0$			$\lambda_{\text{TP}}=0.5$			$\lambda_{\text{TP}}=1$		
	DSC $\uparrow$ (%)	CD $\downarrow$ (mm)	TVS $\downarrow$	DSC $\uparrow$ (%)	CD $\downarrow$ (mm)	TVS $\downarrow$	DSC $\uparrow$ (%)	CD $\downarrow$ (mm)	TVS $\downarrow$
MMWHS	<b>93.6</b>	0.37	0.0411	92.1 (-1.5)	0.22 (-0.15)	0.0093 (-77.4%)	89.2 (-4.4)	<b>0.18</b> (-0.19)	<b>0.0032</b> (-92.2%)
WHS++	<b>91.8</b>	0.68	0.0709	90.6 (-1.2)	0.42 (-0.26)	0.0065 (-90.8%)	88.7 (-3.1)	<b>0.25</b> (-0.43)	<b>0.0049</b> (-93.1%)
ACDC	<b>92.2</b>	0.16	0.0543	90.8 (-1.4)	0.24 (+0.08)	0.0050 (-90.8%)	89.1 (-3.1)	<b>0.20</b> (-0.04)	<b>0.0054</b> (-90.1%)

### 3.2 Results

Tables 1 and 2 demonstrate that TPM Loss significantly reduces topology errors while maintaining competitive segmentation accuracy. Across all datasets, TVS

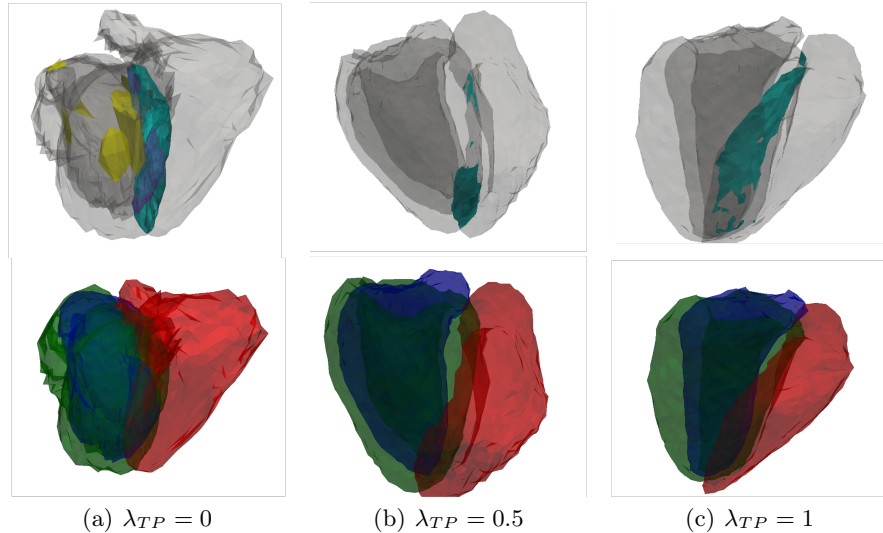


Fig. 2: Effect of topology-preserving loss ( $\lambda_{TP}$ ) on mesh reconstruction, shown across three salient independent cases (one per column) selected under the same hyperparameter. **Top row:** Highlighted regions indicate topology violations. The colors correspond to different types of topology violations, as detailed in Figure 1. **Bottom row:** The reconstructed 3D meshes under different  $\lambda_{TP}$  values.

decreases by 89.7% to 93.1%, confirming its effectiveness in preventing anatomical inconsistencies such as chamber intersections and membrane penetrations. This trend is further illustrated in Figure 2, where the highlighted errors in the top row show severe topology violations when  $\lambda_{TP} = 0$ , which are progressively corrected as  $\lambda_{TP}$  increases, aligning with the quantitative reduction in TVS.

In addition to topology correction, Chamfer Distance improves, with reductions of up to 0.21 mm for CT and 0.26 mm for MRI, indicating that TPM Loss enhances mesh smoothness alongside topological consistency. The bottom row of Figure 2 supports this, where increasing  $\lambda_{TP}$  results in progressively cleaner and more anatomically plausible 3D meshes.

However, enforcing topology constraints leads to a minor trade-off in segmentation accuracy, as reflected in DSC reductions of 1.2% to 4.4%, with the largest drop occurring at  $\lambda_{TP} = 1.0$ . This is expected, as strong topological constraints limit the model’s ability to optimize for pixel-wise accuracy, prioritizing anatomical correctness instead. Nevertheless, the qualitative results in Figure 2 suggest that the reduced DSC does not correspond to degraded anatomical quality, reinforcing that structural integrity is more crucial than marginal segmentation overlap gains.

From Tables 1 and 2, CT benefits most from  $\lambda_{TP} = 0.5$ , while MRI performs better with  $\lambda_{TP} = 1.0$ . CT’s higher spatial resolution and lower shape variability

allow moderate constraints to correct topology errors without distorting anatomical structures. In contrast, MRI exhibits greater anatomical variability and segmentation noise, requiring stronger constraints for topological consistency. Figure 2 (CT results) aligns with this observation, where  $\lambda_{\text{TP}} = 0.5$  provides the best trade-off between geometric accuracy and topology correction, while  $\lambda_{\text{TP}} = 1.0$  further reduces topology errors at the cost of minor over-regularization.

## 4 Conclusions

This paper introduced a Topology-Preserving Mesh Loss (TPM Loss) to enforce anatomical consistency in 3D cardiac mesh reconstruction. Unlike traditional approaches, TPM Loss directly integrates topological constraints at the mesh level, ensuring physiologically plausible structures. Extensive experiments on CT and MRI datasets demonstrate that TPM Loss significantly reduces topology violations—by up to 93.1%—while maintaining competitive segmentation accuracy. As a model-agnostic loss, it can be incorporated into any segmentation-based mesh reconstruction pipeline, regardless of the feature extraction architecture. While this study validates TPM Loss on a 3D U-Net and GCN framework, future research will explore its applicability to transformer-based models and its generalization to other anatomical structures, such as skeletal reconstructions.

## 5 Acknowledgement

Guang Yang was supported in part by the ERC IMI (101005122), the H2020 (952172), the MRC (MC/PC/21013), the Royal Society (IEC\NSFC\211235), the NVIDIA Academic Hardware Grant Program, the SABER project supported by Boehringer Ingelheim Ltd, NIHR Imperial Biomedical Research Centre (RDA01), Wellcome Leap Dynamic Resilience, UKRI guarantee funding for Horizon Europe MSCA Postdoctoral Fellowships (EP/Z002206/1), and the UKRI Future Leaders Fellowship (MR/V023799/1).

I sincerely appreciate the support and invaluable help of a special someone who assisted in the design of the tables, making the data presentation clearer and more effective.

## References

1. Acebes, C., Moustafa, A.H., Camara, O., Galdran, A.: The centerline-cross entropy loss for vessel-like structure segmentation: Better topology consistency without sacrificing accuracy. In: International Conference on Medical Image Computing and Computer-Assisted Intervention. pp. 710–720. Springer (2024)
2. Augustin, C.M., Neic, A., Liebmann, M., Prassl, A.J., Niederer, S.A., Haase, G., Plank, G.: Anatomically accurate high resolution modeling of human whole heart electromechanics: a strongly scalable algebraic multigrid solver method for nonlinear deformation. *Journal of computational physics* **305**, 622–646 (2016)

3. Bernard, O., Lalande, A., Zotti, C., Cervenansky, F., Yang, X., Heng, P.A., Cetin, I., Lekadir, K., Camara, O., Ballester, M.A.G., et al.: Deep learning techniques for automatic mri cardiac multi-structures segmentation and diagnosis: is the problem solved? *IEEE transactions on medical imaging* **37**(11), 2514–2525 (2018)
4. Defferrard, M., Bresson, X., Vandergheynst, P.: Convolutional neural networks on graphs with fast localized spectral filtering. *Advances in neural information processing systems* **29** (2016)
5. Fan, H., Su, H., Guibas, L.J.: A point set generation network for 3d object reconstruction from a single image. In: *Proceedings of the IEEE conference on computer vision and pattern recognition*. pp. 605–613 (2017)
6. Gupta, S., Hu, X., Kaan, J., Jin, M., Mpoy, M., Chung, K., Singh, G., Saltz, M., Kurc, T., Saltz, J., et al.: Learning topological interactions for multi-class medical image segmentation. In: *European Conference on Computer Vision*. pp. 701–718. Springer (2022)
7. Kong, F., Shadden, S.C.: Learning whole heart mesh generation from patient images for computational simulations. *IEEE Transactions on Medical Imaging* **42**(2), 533–545 (2022)
8. Kong, F., Wilson, N., Shadden, S.: A deep-learning approach for direct whole-heart mesh reconstruction. *Medical image analysis* **74**, 102222 (2021)
9. Luo, Y., Sesia, D., Wang, F., Wu, Y., Ding, W., Huang, J., Shi, F., Shah, A., Kaural, A., Mayet, J., et al.: Explicit differentiable slicing and global deformation for cardiac mesh reconstruction. *arXiv preprint arXiv:2409.02070* (2024)
10. Luo, Y., Wang, Y., Xiang, Z., Xiu, Y., Yang, G., Yap, C.: Differentiable voxelization and mesh morphing. *arXiv preprint arXiv:2407.11272* (2024)
11. Maher, G., Wilson, N., Marsden, A.: Accelerating cardiovascular model building with convolutional neural networks. *Medical & biological engineering & computing* **57**, 2319–2335 (2019)
12. Marx, L., Gsell, M.A., Rund, A., Caforio, F., Prassl, A.J., Toth-Gayor, G., Kuehne, T., Augustin, C.M., Plank, G.: Personalization of electro-mechanical models of the pressure-overloaded left ventricle: fitting of windkessel-type afterload models. *Philosophical Transactions of the Royal Society A* **378**(2173), 20190342 (2020)
13. Mittal, R., Seo, J.H., Vedula, V., Choi, Y.J., Liu, H., Huang, H.H., Jain, S., Younes, L., Abraham, T., George, R.T.: Computational modeling of cardiac hemodynamics: Current status and future outlook. *Journal of Computational Physics* **305**, 1065–1082 (2016)
14. Rustamov, R.M., et al.: Laplace-beltrami eigenfunctions for deformation invariant shape representation. In: *Symposium on geometry processing*. vol. 257, pp. 225–233 (2007)
15. Shit, S., Paetzold, J.C., Sekuboyina, A., Ezhov, I., Unger, A., Zhylka, A., Pluim, J.P., Bauer, U., Menze, B.H.: cldice-a novel topology-preserving loss function for tubular structure segmentation. In: *Proceedings of the IEEE/CVF conference on computer vision and pattern recognition*. pp. 16560–16569 (2021)
16. Suinesiaputra, A., Ablin, P., Alba, X., Alessandrini, M., Allen, J., Bai, W., Cimen, S., Claes, P., Cowan, B.R., D’hooge, J., et al.: Statistical shape modeling of the left ventricle: myocardial infarct classification challenge. *IEEE journal of biomedical and health informatics* **22**(2), 503–515 (2017)
17. Trayanova, N.A., Constantino, J., Gurev, V.: Electromechanical models of the ventricles. *American Journal of Physiology-Heart and Circulatory Physiology* **301**(2), H279–H286 (2011)

18. Zhang, C., Guan, W., Xing, X., Yang, G.: Preserving cardiac integrity: A topology-infused approach to whole heart segmentation. arXiv preprint arXiv:2410.10551 (2024)
19. Zhuang, X., Li, L., Payer, C., Štern, D., Urschler, M., Heinrich, M.P., Oster, J., Wang, C., Smedby, Ö., Bian, C., et al.: Evaluation of algorithms for multi-modality whole heart segmentation: an open-access grand challenge. *Medical image analysis* **58**, 101537 (2019)
20. Özgün Çiçek, Abdulkadir, A., Lienkamp, S.S., Brox, T., Ronneberger, O.: 3d unet: Learning dense volumetric segmentation from sparse annotation. In: International Conference on Medical Image Computing and Computer-Assisted Intervention (2016), <https://api.semanticscholar.org/CorpusID:2164893>